Weber, M. E., Tougiannidis, N., Kleineder, M., Bertram, N., Ricken, W., Rolf, C., Reinsch, T., Antoniadis, P. (2010): Lacustrine sediments document millenial-scale climate variability in northern Greece prior to the onset of the northern hemisphere glaciation. - Palaeogeography Palaeoclimatology Palaeoecology, 291, 3-4, 360-370

DOI: 10.1016/j.palaeo.2010.03.007

Lacustrine sediments document millennial-scale climate variability in northern Greece prior to the onset of the northern hemisphere glaciation

Weber[a]*, M.E., Tougiannidis[a], N., Kleineder[a], M., Bertram[a], N., Ricken[a], W., Rolf[b], C., Reinsch[c], T. and Antoniadis[d], P.

[a]Institute for Geology and Mineralogy, Zuelpicher Str. 49a, 50935 Cologne, Germany

[b]Leibniz Institute for Applied Geosciences, OT-Grubenhagen, 37574 Einbeck, Germany

[c]GeoForschungsZentrum Potsdam, Telegrafenberg, 14407 Potsdam, Germany

[d]National Technical University of Athens, Heroon Polytechniou Str. 9, 15780 Zografou-Athens, Greece

*Correspending author.
E-mail address: michael.weber@uni-koeln.de (M.E. Weber)

Revised version (Febuary 2010). Journal – Palaeo 3
8 Figures, ca. 6000 words.

Abstract

We investigated two lignite quarries in northern Greece for orbital and suborbital climate variability. Sections Lava and Vegora are located at the southern and northern boundaries of the Ptolemais Basin, a northwest southeast elongated intramontane basin that contains Upper Miocene to Lower Pliocene lacustrine sediments. Sediments show cyclic alterations of marl-rich (light), and coal-rich or clay-rich (dark) strata on a decimeter to meter scale. First, we established low-resolution ground-truth stratigraphy based on paleomagnetics and biostratigraphy. Accordingly, the lower 67 m and 65 m that were investigated in both sections Vegora and Lava, respectively, belong to the Upper Miocene and cover a time period of 6.85 to 6.57 and 6.46 to 5.98 Ma at sedimentation rates of roughly 14 and 22 cm/ka. In order to obtain a robust and high-resolution chronology, we then tuned carbonate minima (low L* values; high magnetic susceptibility values) to insolation minima.

Besides the known dominance of orbital precession and eccentricity, we detected a robust hemi-precessional cycle in most parameters, most likely indicative for monsoonal influence on climate. Moreover, the insolation-forced time series indicate a number of millennial-scale frequencies that are statistically significant with dominant periods of 1.5 – 8 kyr. Evolutionary spectral analysis indicates that millennial-scale climate variability documented for the Ptolemais Basin resembles the one that is preserved in ice-core records of Greenland. Most cycles show durations of several tens of thousands of years before they diminish or cease. This is surprising because the generally argued cause for Late Quaternary millennial-scale variability is associated with the presence of large ice sheets, which cannot be the case for the Upper Miocene. Possible explanations maybe a direct response to solar forcing, a influence on the formation of North Atlantic Deep Water through the outflow of high-salinity water, or an atmospheric link to the North Atlantic Oscillation.

Keywords: cyclic processes; orbital forcing; millennial-scale climate; paleomagnetics; non-destructive data sets; insolation; Greece

Introduction and Rationale

Since the pioneering work of Hays et al. (1976) and Imbrie et al. (1984) it has been proved that cyclic changes in the earth orbital parameters (Milankovitch, 1941), namely eccentricity (413 kyr, 123 kyr, 95 kyr), obliquity (41 kyr), and precession (19 kyr, 23 kyr), led to changes in the earth energy budget that were large enough to be preserved in marine sediments. Theoretical calculation of Berger (1976) and Berger and Loutre (1991) supported their concept. Henceforth, cyclic variability in sediment strata was used to develop detailed orbital chronologies.

Magnetic polarity stratigraphy is an excellent and independent tool to retrieve chronometric information. It is based on polarity changes of the Earth's magnetic field as documented in the geomagnetic polarity timescale (GPTS, Cande and Kent, 1995). Langereis and Hilgen (1991) and Hilgen et al. (1995) provided the first astronomical age scale for the Pliocene Capo Rosello sections in Sicily based on the GPTS. Their work was further substantiated by Krijgsman et al. (1995).

A low-resolution, orbital-based chronology for the continental Ptolemais Basin was introduced by Steenbrink et al. (1999) and van Vugt et al. (1998; 2001). They ascribed cyclic changes of carbonates and lignites to orbital variability: maxima in lake carbonate correlate to maxima in insolation (and minima in precession). Accordingly, lignite maxima correlate to minima in insolation (i.e., beige layers in Capo Rosello). Also, they carried out extensive physical dating using $^{40}Ar/^{39}Ar$ (e.g., Kuiper, 2003) and delivered a high-quality composite

stratigraphy for the Ptolemais Basin (Steenbrink et al., 2006). Therefore, there is a robust and reliable low-resolution magnetic stratigraphy we could base our investigations on.

Millennial-scale variability ranges in the suborbital frequency band and has proved to be a persistent climate element in the Late Quaternary, where it is typically associated with large continental ice sheets (Bond et al., 1992; Dansgaard et al., 1993; Bond and Lotti, 1995), as well as in earlier times (e.g., Bartoli et al., 2005). As for the Ptolemais Basin, Kloosterboer-van Hoeve et al. (2006) found millennial-scale variability in a pollen record covering one precession cycle. Also, Steenbrink et al. (2003) found indication for millennial-scale fluctuations in a color reflectance record over one eccentricity cycle.

So far, there is no high-resolution record that would cover a large portion or even the entire lignite/carbonate alteration in the Ptolemais Basin. Our goal therefore was to collect high-resolution and continuous paleoclimate proxy data to reconstruct both orbital and suborbital climate change through time by analyzing two Upper Miocene quarries (Lava and Vegora) in northwestern Greece. We generated multiproxy data (sediment color, magnetic susceptibility, and natural gamma) to gain differentiated insight into past climate variability during a time prior to the onset of northern hemisphere glaciation.

Figure 1 should be placed here

Location and setting

The Ptolemais Basin (Fig. 1) is a SSE – NNW elongated Basin that formed during the Late Neogene in northwestern Greece (Pavlides and Mountrakis, 1987). It contains a limnic archive of Upper Miocene to Quaternary continental strata (up to 800 m thick; Anastopoulos and Koukouzas, 1972) with an extended Lower Pliocene alteration of lignites and carbonates. The depositional history reflects interaction of orbital forcing and tectonic movement

(Steenbrink et al., 2006). Through continued Pleistocene extension, the Basin is further subdivided into the basins of Florina-Vevi, Amynteon-Vegora, Ptolemais, and Kozani-Servia (Antoniadis et al., 1994), which comprise a number of active coal mining fields (Tougiannidis, 2009) and outcrops. The deposits are highly fragmented due to fault tectonics.

The Vegora section in the north (Amynteon-Vegora Sub-Basin) and the Lava section in the south (Kozani-Servia Sub-Basin) are the focus of this paper (Fig. 1). Stratigraphically, both belong to the Komnina Formation. The Komnina Formation is divided into the lowermost Servia-Member, followed by the Lava member and concluded by the Prosilio member. Both outcrops investigated here, belong to the Lava member. These fluvial, deltaic, and limnic deposits overlie the pre-Neogene basement of the Pelagonian Zone. Transgression during the Upper Miocene favored conditions for coal marsh formation in the limnic Kozani-Servia-Basin and led to the formation of the Komnina Formation.

Section Vegora

The open-pit mine of Vegora (latitude 40° 42’ N, longitude 21° 44’ E) is located at the southwestern edge of the Vegoritis Lake. It is about 1 km^2 in size and has been abandoned in the year 2000. A detailed description can also be found in Steenbrink et al. (2006). Due to access restrictions, only the lowermost 67 m of the section was investigated (see Fig. 2a). The lowermost unit contains 1.5 m thick gray marls, followed by a 8.5 m thick xylit layer. The unit above is 30 m high and contains clayey marls intercalated with silty to sandy fossil-rich layers, and a 1-m thick sandy conglomerate at the top. The uppermost unit is 26 m high and consists of gray to beige marl to clay that is rich in plant fragments, diatoms and ostracods. Occasionally, there are taphocoenosis of diatom-rich sections, which can be considered diatomites. The uppermost unit is completed by a 3-m thick fining upward conglomerate

sequence. Above the section investigated in detail, there are 11 m of clayey marls with sandy layers. Velitzelos and Gregor (1990) confirmed the age of the lignites by plant relics. Steenbrink et al. (2006) dated the marls using $^{40}Ar/^{39}Ar$. Above that, there are 52 m of altering laterites, conglomerates and clayey marls, presumably belonging to the Prosilio member (see Fig. 2a).

Section Lava

The Lava section is located in an active lignite quarry of the small village Lava (latitude 40° 16' N, longitude 21° 57' E), which is about 100 kilometers southwest of Thessaloniki and a few kilometers south of Servia (longitude 21,95°E, latitude 40,26°N; Fig. 1). A detailed description can also be found in Steenbrink et al. (2000). Access restrictions allowed for detailed sampling only from 0 to 65 m (see Fig. 2b). The lowermost part is 12 m thick and contains two lignite seams of 5 m and 4 m thickness, respectively. Both seams show zebra structures, i.e., lignite alternates with conglomerate, sand, clay, and marl (Tougiannidis, 2009). Specifically the lower seam is enriched in xylit. The two seams are separated by a 3-m thick marl-clay-sand alteration. This lower Komnina Formation was dated as Late Miocene using mammalian fossils (*Tetralophodon longirostris*; KAUP, 1832), plant remnants, and charophytes (Antoniadis et al., 1994; Steenbrink et al., 2000).

The section above contains 7 m of light green to olive green clay marls, which are overlain by 12 m of cyclically bedded gray clayey marls. The next section is 22 m thick and alteration of cm- to dm-thick lignite horizons, gray to green clay marls, and brown clays. The upper 9 m consists primarily of gray marls and cm-thick clay horizons.

Figure 2 should be placed here

Methods

The methods of this study rely primarily on high-resolution non-destructive investigations that have been accomplished with a number of tools. The measurements were done on clean and fresh (scraped with a spatula) surfaces. A total of approximately 13,200 color measurements were carried out with a Minolta Chromatometer CM—2002 at 1-cm increments, using the so-called "L*-a*-b*" color system which provides three color values for each measurement: The L* axis is the black-white color component, known as lightness or grey value. The a*axis is the green/red component and the b*axis is the yellow/blue component (details see Weber, 1998). Together, the three parameters describe coordinates in a spherical system (16 million possible variations). The difference between two successive color coordinates (ΔE^*ab) was calculated as $\Delta E^*ab = \sqrt{(\Delta L^*)^2 + (\Delta a^*)^2 + (\Delta b^*)^2}$. Since ΔE^*ab contains the variability of all three color components, we refer to it as the whole color difference.

Natural gamma radiation was measured with a gamma-scintillometer and a broadband sensor. The conversion from the measured counts per second (cps) to the international standard API was achieved by using the formula API=12*2.2*NGR (cps). The broadband sensor measures gamma-ray in an energy-field from 60 KeV to 2.8 MeV. To find the appropriate balance between speed and data quality, we chose a measurement time of ten seconds and averaged two analyses. The measurement increment was 6 cm. The same increment was chosen for magnetic susceptibility measurements, which were achieved with a mobile kappameter. Accordingly, we collected a total of roughly 2,200 measurements for natural gamma and magnetic susceptibility.

Paleomagnetic measurements were made on discrete samples in the lab. We determined natural remanent magnetization (NRM) and alternating-field demagnetization (AF). These

measurements were used to generate the characteristic remanent magnetization (ChRM) (see Fig. 3). A total of 180 samples were retrieved at 50-cm intervals on average. We used completely oriented diamagnetic sample cubes of 12 cm^2. Remanent magnetization was measured in x and y direction using a cryogenic spin magnetometer (2G Enterprises). We applied alternating-field demagnetization (AF) before inclination and declination was measured. Using orthogonal projections (Zijderveld, 1967), we corrected the values for noise before using them for magnetostratigraphy.

We used Analyseries software (Paillard et al., 1996) to perform astronomical tuning experiments and to construct age-depth models. Orbital parameters for the time frame 7 – 6 Ma were calculated in 1 kyr increments for eccentricity, obliquity, precession, using the solutions provided by (Laskar et al., 2004). Orbital insolation was calculated for the month of June at 40°N to reflect the energy budget of the site.

To achieve comparable results for the analysis of suborbital frequencies, data in the time domain were first pre-treated in several ways. The average sample resolution for sediment color is roughly 43 yr for section Lava and 76 cm for section Vegora. Therefore, we re-sampled those data sets every 40 and 80 yr, respectively. The average sample resolution of magnetic susceptibility and natural gamma is roughly 258 and 456 yr, which have been re-sampled at 250 and 450 yr, respectively, for sections Lava and Vegora. Then we applied a 3-point smoothing to all data sets to eliminate high-frequency noise. Finally, we suppressed the orbital amplitude (which is mostly the dominant signal) by applying a high-pass filter of 0.1 cycles/kyr to the data sets, so that only periods shorter than 10 kyr are visible in the spectra.

In order to study the resulting time series for frequency pattern and to compare them to orbital time series, we developed a software package called ESALAB to conduct both bulk and evolutionary spectral analysis (ESA). This program relies on the Lomb (1976) and

Scargle (1982; 1989) algorithms, which provide an estimate of the spectrum by fitting harmonic sine and cosine components to the data set. It has two decisive advantages: the input data can be unequally spaced and the resulting spectra are robust and of high resolution. For the Fourier transformation, window length and step size are adjustable, and the window type is selectable among Hanning, Haming, Blackman, $\sin^2$, and boxcar. Besides the data, the output consists of graphic files for bulk and ESA spectra. With a sample increment of 1 cm, the Nyquist frequency is 0.5 cm^{-1}, i.e., the spatial resolution is 2 cm for spectral analysis.

Results

Ground-truth stratigraphy

We established ground-truth stratigraphy for section Lava first by conducting paleomagnetic measurements (see Table 1). Section Lava shows very stable inclination and declination values. Only at 29 m there is a distinct change in polarity (Fig. 3a), which must be associated with the lower boundary of chron C3An.2n. According to the spreading-rate age scale of Krijgsman et al. (1999), which was specifically designed for this time slice, this reversal is 6.731 Ma old.

Table 1 should be placed here

To obtain additional ground-truth stratigraphic information, we compared our survey to the one that has been carried out by (Steenbrink et al., 2000). This was not an easy or straightforward task since the surveys haven't been carried out at the exact same locations and the conditions in the outcrop have changed over the years. However, the fossil findings at the top of our section in 63 m could be correlated to "key bed II" of their study; those from 27 m depth to "key bed I". Three further age control points could be taken confidently to match their tuning points (option 1) for cycles 1, 4, and an unnamed cycle underneath "key bed II",

in 18, 48, and 60 m, respectively (see Table 1 for details). As a result, sedimentation rates are fairly constant (22 – 23 cm/ka). Only the topmost section (above 60 m) decreases to 14 cm/ka. This finding is consistent with the interpretation of Steenbrink et al. (2000), who also argued for a decrease close to the top of the section that we have studied.

Figure 3 should be plfreitaced here

Section Vegora shows a much more scattered paleomagnetic pattern (Fig. 3b). The correlation to the polarity time scale of Krijgsman et al. (1999) reveals chron C3An.2n (6.37 Ma) at the base of the section with normal polarity. Since the xylite-rich seam in the lower part could not be used for paleomagnetic measurements, we follow the interpretation of (Steenbrink et al., 2006), who determined the top of chron C3An.2n just above the seam based on one sample, where we determined scattered data (in 12.73 m depth). Another interval of normal polarity was detected between 24.96 m and at 61.44 m, indicating the base and top of chron C3An, with ages of 6.28 Ma and 6.1 Ma, respectively. We took these three age control points for the low-resolution age model of section Vegora (see Table 1). Comparison reveals systematically thicker sediments for the survey of Steenbrink et al. (2006). This could be due to lateral thickness variability in facies, or, more likely, mistakes in measuring the thicknesses in the outcrop when changing from one terrace to another.

To summarize the ground-truth stratigraphy, the measured samples from section Lava cover a period from 6.85 to 6.57 Ma, whereas section Vegora covers a period from 6.46 to 5.98 Ma. Accordingly, section Vegora is stratigraphically younger than section Lava, and both represent an Upper Miocene succession of almost 900 kyr with a gap of roughly 110 kyr.

Cyclic variability of high-resolution non-destructive data

A total of six sediment-physical and optical data sets (L*, a*, b*, ΔE*ab, magnetic susceptibility, and natural gamma) were either measured non-destructively or derived indirectly. Most of them characterize facies changes and show striking cyclic variability (Figs. 4 and 5); others may remain rather complex or inconclusive. The advantage of using a number of different climate proxy records is that various aspects of changing sediment composition and supply and the relation to climate forcing can be addressed simultaneously.

Figure 4 should be placed here

Specifically sediment lightness shows a striking pattern in both sections with brighter (marl-rich) and darker (clay-rich or coal-rich) intervals, and the coal seams as the darkest parts. Therefore, L* is generally a good indicator for either calcium carbonate contents (see also Weber, 1998) or organic carbon.

The whole color difference ΔE*ab also reveals a very striking pattern of both low- and high-frequency variability, in the orbital and millennial frequency band, respectively. Both sections show high-amplitude internal variations and elevated values within the coal seams (Figs. 4 and 5). Only section Lava displays an overall decrease toward the top.

For section Vegora, b* values show an increase within the beige marls between 40 m and 60 m (Fig. 5). Higher b* values reflect elevated contents of yellowish iron oxides as indicated by the presence of hematite and goethite for the upper part of section Vegora. Low b* values refer to bluish components, abundant in bitumen or coal (e. g., the upper seam of section Lava at 10 m (see Fig. 4), or provided by sulfides.

The variation between red and green sediment – color value a* – provides an indication for the redox conditions, although the signal might be influenced by secondary (diagenetic) overprint. For section Vegora, there is a certain similarity between color values a* and b*,

specifically for the increase within the beige marls caused by higher contents of iron oxides. However, for section Lava, there is no striking correlation between a* and b*.

Gamma-ray logs provide a measurement for the amount of radioactive elements. Specifically within expansive clay minerals, radioactive elements accumulate. Hence, the gamma-ray log can be used as a grain-size indicator with lower contents in coarser (sandier) sediment. Accordingly, section Vegora shows a number of distinct coarsening up and fining up cycles, whereas section Lava reveals a less distinct pattern. Marl-rich sediment usually shows lower gamma values. For the coal seams, the two sections show opposite trends. While section Vegora shows minimum gamma-ray values, section Lava displays elevated values in the lowermost 8 m, calling for an additional sediment supply source containing radioactive elements. Uranium, for instance, could then be absorbed by the organic components of the lignite.

Magnetic susceptibility measurements give an estimate of the extent to which sediments may be magnetized. Usually, clay-rich sediment exhibits higher magnetite contents and hence, magnetic susceptibility is enhanced. Generally, both sections display low-amplitude, high-frequency variability. Values for section Lava are about an order of magnitude higher on average than those for section Vegora. Specifically within the coal seam of section Vegora, values are low.

Figure 5 should be placed here

Astronomical tuning

The tuning process provides the quantitative correlation of the cyclic lignite marl alterations to orbitally-calibrated time series according to Laskar et al. (2004), using the climate proxy records described above, and relying on the magnetic polarity time scale of

Krijgsman et al. (1999) as ground-truth stratigraphy. Accordingly, we first generated low-resolution age models for sections Lava and Vegora by using the stratigraphic fix points of Table 1 (see blue dots in Fig. 6). These first age models are sufficient to conduct spectral analysis in order to study the relative contribution of individual orbital frequencies.

The highest orbital frequency present in the Ptolemais Basin is the precession cycle (Steenbrink et al., 1999). Pollen studies of Steenbrink et al. (2000) in the Lava section showed that dark-colored marls correspond to relatively dry periods, whereas light-colored marls represent more humid periods. Since humid climate in the Mediterranean occurred during insolation maxima (e.g., Emeis et al., 2000), we used the insolation curve for the month of June at 40°N according to Laskar et al. (2004) and tuned individual carbonate minima to insolation minima. Thereby, we increased the resolution of the age models without violating the boundaries provided by Table 1. Depending on which of the proxy records we used, this procedure provided between 14 and 24 additional age control points. Since we followed the strategy of Steenbrink et al. (2000; 2006) of tuning insolation minima to dark intervals, we obtained about the same resolution in the tuned age models as they did. The tuning offers a certain degree of freedom, so that the resulting age scales may differ slightly from one parameter to another. However, the established correlation between climate proxy variability and orbital parameter is striking, specifically for magnetic susceptibility and L* (Fig. 6). In most cases, the tuning revealed two carbonate peaks for every insolation cycle, a fact that has also been found in other records (Vollmer et al., 2008). As a whole, we are confident that our method provides a sound high-resolution age model with fix points at (ideally) all insolation minima.

Figure 6 should be placed here

The resulting age-depth relationship is rather uniform for section Vegora (Fig. 6 center), implying relatively stable conditions. Sedimentation rates range from 13 to 16 cm/kyr with and average of 14 cm/kyr, which is less than the 18 cm/ka deduced by Steenbrink et al. (2006), a difference that has already been discussed for the ground-truth stratigraphy (Table 1). Accordingly, eccentricity cycles occur roughly every 14 m, obliquity cycles every 6 m, and precession cycles every 3 m. Section Lava has higher sedimentation rates (20 – 25 cm/kyr, averaging 22 cm/kyr), except for the top part (above 60 m, younger than 6.59 Ma), where sedimentation rates decrease to roughly 14 cm/kyr. So for most part of the section, eccentricity cycles occur every 22 m, obliquity cycles every 9 m, and precession cycles every 4.5 m. The overall sedimentation rate difference between sections Lava and Vegora implies that the northern boundary of the Ptolemais Basin received about one third less of sediment than the southern boundary during the Upper Miocene.

Spectral analysis

Initial spectral analysis in the depth domain showed some cyclic behavior of most proxies with average cycle length of about 4.5 to 5 m for section Lava and 2.5 to 3 m for section Vegora. However, spectral analysis in the depth domain remains ambiguous because slight changes in sedimentation rate might diminish the amplitude of the response beyond recognition. Therefore, we consider this only qualitative information. We believe that depth series should first be transformed into the time domain using (with solid age control points) before spectral analysis and orbital tuning are conducted, specifically if many high-resolution proxies have been measured and can hence be used for the process.

Since we used orbital parameters as tuning targets, these frequencies are obviously present in bulk spectra. Orbital precession is most dominant, since it contributes a substantial

part to the insolation forcing in low-to-mid latitudes. Orbital eccentricity modulates the amplitude of the precession cycle (Imbrie et al., 1993) and is therefore also significant for the Ptolemais Basin (Steenbrink et al., 2006), specifically in the lower sedimentation-rate sites of the Ptolemais Basin (Tougiannidis, 2009). Obliquity has only a minor impact, which is not surprising since this frequency is mainly dominant at higher latitudes (e.g., Weber et al., 2001), where it is mostly associated with the presence of larger ice sheets (e.g., Ruddiman, 2004). Compared to our results, Steenbrink et al. (2006) found a more robust obliquity cycle in some parts of section Lava. However, our study focuses on the suborbital frequency band, where, so far, no study is available at high resolution and over longer time scales.

The study of suborbital frequencies requires high-resolution, at least precession-forced age models. Without the 20 kyr control, spectral power in the suborbital frequency band is not persistent enough over longer time scales (for instance when only ground-truth stratigraphy is applied). On the other hand, when precession tuning is applied, a number of significant millennial-scale frequencies are detectable in evolutionary spectra.

Figure 7 should be placed here

Several important findings should be pointed out. First, apparently there is no centennial-scale variability preserved. Even unsmoothed color time series in the lower part of section Lava did not show any spectral power, although the temporal resolution would be more than sufficient (i. e., 40 to 50 yr). However, rhythmic bedding in the cm to dm band can be observed in the outcrop. Either this type of bedding is not cyclic, or, more likely, post-sedimentary compaction operates different on the various facies types, thereby altering the depth-age relationship that has originally been established. Because the age control points are only precession-controlled at best, this issue cannot be resolved here.

Second, all data sets reveal the presence of millennial-scale frequencies. In most cases bulk spectra indicate significant variability every 1 to 8 kyr. Third, opposed to orbital-scale frequencies, millennial-scale cycles are not persistent throughout the record. Rather, they occur over several tens of thousands of years before decrease in amplitude or disappear.

Discussion

Cyclic changes in color between marl-rich (light) and clay-rich or lignite-rich (dark) sediment indicate periodic changes in humidity. The sites are located in a continental setting at low- to mid-latitudes. Here, insolation changes as the ultimate driver of humidity changes have a strong precessional component. Sediments were deposited in shallow water (van de Weerd, 1983; Kaouras, 1989) of an intramontane lacustrine basin. The coal formation at the base of section Lava started at approximately 7 Ma. During this time the dominantly marly successions in Sicily changed to diamictites. The diatomite formation south of Crete followed with a 200-300 yr time lag. Between 7 Ma and 6 Ma both, northwestern Greece and the marine Mediterranean were affected by a decrease of ferrigenous sediment supply (Steenbrink et al., 2006). According to the pollen studies of Kloosterboer-van Hoeve et al. (2006) dark-colored marls of the Ptolemais Basin, which are mostly enriched in clay and/or organic carbon, correspond to relatively dry periods, whereas light-colored marls represent more humid periods. During the Messinian Salinity Crisis (Upper Miocene; Butler et al., 1999), slab tectonic events led to the closure of the straight of Gibraltar. As a result of the separation of the Atlantic Ocean from the Mediterranean Sea, sea level dropped several km until approximately 6 Ma (Krijgsman et al., 1999), when evaporitic sediment precipitated in the oceanic basin and the Prosilio member established in the Ptolemais Basin with fluvial and alluvial deposits at section Vegora (above the interval investigated here). Exactly at that time,

the limnic depocenter must have shifted away from the boundaries of the Ptolemais Basin as documented by the termination of deposition at site Vegora.

The presence of a hemi-precession cycle in L* time series of the Ptolemais Basin has also been documented by Steenbrink et al. (2003). It could point to an increased monsoonal influence. Since higher L* values indicate elevated carbonate content, there must have been two carbonate precipitation events over the course of one precession cycle. Hemi-precession carbonate cycles have, for instance, been described by Vollmer et al. (2008) for Triassic playa sediment that has been deposited under monsoonal influence. The two carbonate precipitation events were most likely created when equinoxes were in perihelion and aphelion, respectively. Sun and Huang (2006) found hemi-precession cycles in Chinese loess during interglacial times, when northern hemisphere ice shields were small. During those times, the response to obliquity was diminished and the summer monsoon reached further north.

Millennial-scale climate cycles are well known from Late Quaternary ice cores from Greenland (Dansgaard et al., 1993), where they are called Dansgaard-Oeschger cycles (DO), or from Antarctica (Epica community members, 2006), where they are referred to as Antarctic Isotopic Maxima (AIM). The main frequency here is 1.5 kyr (Bond et al., 1997) and, specifically for the northern hemisphere, groups of 3 to 5 cycles form so-called Bond cycles with periods from approximately 5 to 9 kyr. At the end of a Bond cycle, massive iceberg calving occurred in the North Atlantic, the so-called Heinrich events (Bond et al., 1992). These were peak cold times with significantly reduced production of North Atlantic Deep Water and cold climate in Europe. Subsequent melting led to a massive freshwater signal in the North Atlantic (Broecker, 2000), before abrupt temperature rise led to strengthening of the thermohaline convection in the North Atlantic and to warmer temperatures in Europe. Accordingly, the spectral evolution of millennial-scale frequencies in the $\delta^{18}O$ record of the

GRIP ice core (data from Grootes et al., 1993) shows a concentration of spectral power between 3 and 8 kyr (Fig. 8b) with a minor impact of 1.5 kyr. The evolutionary spectrum reveals that these cycles are not persistent throughout the record. This is not surprising since the duration between Heinrich events (and thereby Bond cycles) has a tendency to shorten during the last glacial cyle. Specifically during Marine Isotopic Stage (MIS) 3 the presumed threshold in the North Atlantic freshwater balance was crossed regularly (Stocker, 1998), so that the 1.5 kyr cycle occurred consistently over 30 to 40 kyr, whereas before and after, lower millennial-scale frequencies prevail.

Figure 8 should be placed here

For the Ptolemais Basin, indication for the presence of millennial-scale frequencies have been found for short time series (Steenbrink et al., 2003; Kloosterboer-van Hoeve et al., 2006). Our climate proxy records show, for the first time, substantial millennial-scale variability between 1.5 and 8 kyr over the entire time of preservation. As in Greenland, specific cycles last for several tens of thousands of years before they diminish or fade (Fig. 8a). The northern hemisphere did not experience massive glaciation until the Upper Pliocene around 2.8 – 2.5 Ma (e.g., Tiedemann et al., 1994), or between 3.6 and 2.4 Ma (Mudelsee and Raymo, 2005) as recently argued. Hence, the Upper Miocene sections investigated here were unlikely influenced by glaciation. Therefore, the similarity between the Late Quaternary climate record of Greenland ice and the one preserved in northern Greece lacustrine sediment may either be coincident or there is a common underlying cause that cannot be attributed to the presence and processes associated with large ice sheets. If the latter is true, the Late Quaternary millennial-scale variability might not associated with ice sheets at all; instead, it might be a general mode of climate variability.

The major millennial-scale cycle dominating the glacial record of Greenland ice is the 1.5 kyr cycle. We also found the 1.5 kyr cycle in sections Vegora and Lava. As commonly argued (e.g., Bond et al., 1997), this cycle should be associated with large ice sheets. On the other hand, recent modeling studies (e.g., Braun et al., 2005) argue that the 1.5 kyr cycle might be a solar cycle, resulting from the interplay of the Gleisberg (roughly every 85 – 90 yr) and the deVries (roughly every 200 – 220 yr) cycles. Their model produced the 1.5 kyr cycle when forced by periodic freshwater input into the North Atlantic every 87 and 210 yr. In other words, a substantial part of the millennial-scale climate variability might have an external (solar) source. This would be a process that could link Atlantic and eastern Mediterranean climate without invoking large ice sheets because freshwater flux at the surface is directed from the Atlantic into Mediterranean (Robinson et al., 1993), whereas the outflow of high-salinity intermediate and deep waters from the Mediterranean, in turn, has an impact on the formation of North Atlantic Deep Water by delivering the required enhanced salinity. Kloosterboer-van Hoeve et al. (2006), on the other hand, concluded that changes in pollen associations could be linked to the North Atlantic Oscillation (NAO), with a more positive NAO during winter, leading to drier atmospheric conditions in northern Greece, and a more negative NAO in summer, leading to wetter conditions in the eastern Mediterranean (Hurrell, 1995), because atmospheric moisture transport from the Atlantic takes a more southern trajectory during these times. Future research will have to solve the question which of the proposed teleconnections had the largest impact.

Acknowledgments

We thank the Public Power Corporation for granting permission to work in their quarries. We are grateful to T. Apostolikas (Larco) to grant access to section Lava. Also, we

wish to thank T. Perraki and I. Oikonomopoulos (University of Athens) as well as H. Cieszynski and C. Illing (University of Cologne) for analytical assistance. J. Steenbrink and N. van Vugt provided very helpful reviews. M.E.W. was supported by the Deutsche Forschungsgemeinschaft (DFG; grant We2039/2-1). All data of this paper will be made available at the PANGAEA Network for Geological and Environmental Data (thanks to H. Grobe, M. Diepenbrook, and R. Sieger) hosted by the Alfred-Wegener-Institute for Polar and Marine Research (http://www.pangaea.de/home/mweber/).

Figure Captions

Figure 1. Location map of the Ptolemais Basin in northern Greece, containing the Florina, Ptolemais, and Kozani Sub-Basins. Research sections Lava and Vegora (red stars) are located at the southern and northern boundaries, respectively. Basic stratigraphy and lithology is shown to the right. Modified after Papakonstantinou (1979) and van de Weerd (1983).

Figure 2. Photographs from sections Vegora (top) and Lava (bottom). Both show Upper Miocene lignites and marls. For location see Figure 1.; Pr mb = Prosilio Member; Lv mb = Lava Member

Figure 3. Sediment color, lithology, inclination, and declination of sections Vegora (left) and Lava (right). Age assignations to Chron C3An.2n and C3An.1n are according to age scale of Krijgsman et al. (1999). The grey star in section Vegora (left) refers to $^{40}Ar/^{39}Ar$ data determined by Steenbrink et al. (1998).The orange star in section Lava (right) represent stratigraphic marker bed (key bed I, according to Steenbrink et al., 2000). Black stars represent polarity changes. Bone-like object at top (key bed II) of section Lava refers to mammal fossil (right Tibia-Fragment of a *Cervidae*, pers. com. Prof. W. von Koenigswald) finding (Tougiannidis, 2009). Note that the two sections combined provide an almost continuous Upper Miocene record between 6.9 Ma (bottom of section Lava) to 6 Ma (top of section Vegora).

Figure 4. Non-destructive data from section Lava. From left to right are color, lithology, sediment lightness (L*), red-green component (a*), yellow-blue component (b*), whole color difference (ΔE*ab), magnetic susceptibility, and natural gamma. Note that L* provides an estimate for either organic carbon or carbonate; a* indicates the redox state, and b* yields information about the iron oxide content. Shaded areas refer to coal seams.

Figure 5. Non-destructive data from section Vegora. From left to right are color, lithology, sediment lightness (L*), red-green component (a*), yellow-blue component (b*), whole color difference (ΔE*ab), magnetic susceptibility, and natural gamma. For further explanation see Figure 4.

Figure 6. Sediment lightness (L*) and magnetic susceptibility records from section Vegora (left) and Lava (right) tuned versus orbital insolation at 40°N for the month of June (data from Laskar et al., 2004). Note that carbonate minima (magnetic susceptibility maxima) were tuned to insolation minima according to the procedure introduced by Steenbrink et al. (2000, 2006). Center panel gives age depth relationships for the two sections. Note that blue points results from ground-truth stratigraphy given in Table 1, whereas red points are additional insolation tuning points.

Figure 7. Spectral analysis of color component L* for sections Vegora (left) and Lava (right). Bulk spectra (top) were calculated using REDFIT software (Schulz and Mudelsee, 2002). Red line shows the 90 % confidence interval. Evolutionary spectral analyses (bottom) were calculated with ESALAB software (see chapter methods) with a window size of 50 kyr and a shift of 5 kyr from one analysis to the next.

Figure 8. Spectral analysis for the central part of section Lava (left) and for the GRIP ice core (right) from Greenland. Bulk spectra (top) were calculated using REDFIT software (Schulz and Mudelsee, 2002). Red line shows the 90 % and 95 % confidence interval. Evolutionary spectral analyses (bottom) were calculated with ESALAB software (see chapter methods) with a window size of 20 kyr and a shift of 2 kyr from one analysis to the next.

Table Captions

Table 1. Ground-truth stratigraphy for sections Lava (top) and Vegora (bottom). Ages of magnetic reversals rely on Krijgsman et al. (1999); correlation points on Laskar (2004). Section Lava has been correlated to cycles determined by Steenbrink et al. (2000); section lava to those determined by Steenbrink et al. (2006).

Section	Depth (m) Steenbrink et al. (2000)	Depth (m, this study)	Remark	Age (Ma)	Sedimentation rate (cm/ka)
LAVA	27.8	18	Cycle 1	6.780	0.23
	41.8	27	Key bed I	6.740	0.22
	44.2	29	C3An.2n (o)	6.731	0.22
	57.8	48	Cycle 7	6.646	0.23
	69.8	60	Unnamed cycle	6.594	0.14
	73.5	63	Key bed II	6.572	0.14
	Steenbrink et al. (2006)				
VEGORA	73.5	61.44	C3An.1n (t)	6.010	0.14
	37.5	24.96	C3An.1n (o)	6.280	0.14
	16.5	12.73	C3An.2n (t)	6.370	0.14

Literature Citation

Anastopoulos, J. and Koukouzas, C.N., 1972. Economic geology of the southern part of the Ptolemais lignite basin (Macedonia,Greece). Geol. Geophys. Res., 16(1): 1-189.

Antoniadis, P.A., Blickwede, H. and Kaouras, G., 1994. Petrographical and Palynological analysis on a part (36,0 m – 51,0 m) of a Borehole of the Upper Miocene lignite deposit of Lava-Kozani, N.W. Greece Mineral Wealth, 91: 7-17.

Bartoli, G., Sarnthein, M., Weinelt, M., Erlenkeuser, H., Garbe-Schönberg, D. and Lea, D.W., 2005. Final closure of Panama and the onset of northern hemisphere glaciation. Earth and Planetary Science Letters, 237: 33-44.

Berger, A.L., 1976. Obliquity and precession for the last 5,000,000 years. Astron. Astrophys, 51: 127-135.

Berger, A.L. and Loutre, M.-F., 1991. Insolation values for the climate of the last 10 million years. Quaternary Sci. Res., 10: 297-317.

Bond, G., Heinrich, H., Broecker, W., Labeyrie, L., McManus, J., rews, J., Huon, S., Jantschik, R., Clasen, S., Simet, C., Tedesco, K., Klas, M., Bonani, G. and Ivy, S., 1992. Evidence for massive discharges of icebergs into the North Atlantic ocean during the last glacial period. Nature, 360: 245-249.

Bond, G., Showers, W., Cheseby, M., Lotti, R., Almasi, P., deMenocal, P., Priore, P., Cullen, H., Hajdas, I. and Bonani, G., 1997. A Pervasive Millennial-Scale Cycle in North Atlantic Holocene and Glacial Climates. Science, 278: 1257-1266.

Bond, G.C. and Lotti, R., 1995. Iceberg Discharges Into the North Atlantic on Millenial Timescales During the Last Glaciation. Science, 267(5200): 1005-1010.

Braun, H., Christl, M., Rahmstorf, S., Ganopolsky, A., Mangini, A., Kubatzki, C., Roth, K. and Kromer, B., 2005. Possible solar origin of the 1.470-year glacial climate cycle demonstrated in a coupled model. Nature, 438: 208-211.

Broecker, W.S., 2000. Abrupt climate change: causal constraints provided by the paleoclimate record. Earth Planet. Sci Lett., 51: 137-154.

Butler, R.W.H., McClelland, E. and Jones, R.E., 1999. Calibration the duration and timing of the Messinian salinity crisis in the Mediterranean: linked tectonoclimatic signals in thrust-top basins of Sicily. Journal of the Geological Society, 156: 827-835.

Cande, S.C. and Kent, D.V., 1995. Revised calibration of the geomagnetic polarity timescale for the Late Cretaceous and Cenozoic. Journal of Geophysical Research, 100(B4): 6093-6095.

Dansgaard, W., Johnsen, S.J., Clausen, H.B., Dahl-Jensen, D., Gundestrup, N.S., Hammer, C.U., Hvidberg, C.S., Steffensen, J.P., Sveinbjörnsdottir, A.E., Jouzel, J. and Bond, G., 1993. Evidence for general instability of past climate from a 250-kyr ice-core record. Nature, 364: 218-220.

Emeis, K.-C., Sakamoto, T., Wehausen, R. and Brumsack, H.-J., 2000. The sapropel record of the eastern Mediteranean Sea - results of Ocean Drilling Program Leg 160. Palaeogeography, Palaeoclimatology, Palaeoecology, 158: 371-395.

Epica community members, 2006.

Grootes, P.M., Stuiver, M., White, J.W.C., Johnsen, S. and Jouzel, J., 1993. Comparison of oxygen isotope records from GISP2 and GRIP Greenland ice cores. Nature, 366: 552-554.

Hays, J.D., Imbrie, J. and Shackleton, N.J., 1976. Variations in the Earth's Orbit: Pacemaker of the Ice Ages. Science, 194(4270): 1121-1132.

Hilgen, F.J., Krijgsman, W., Langereis, C.G., Lourens, L.J., Santarelli, A. and Zachariasse, W.J., 1995. Extending the astronomical (polarity) time scale into the Miocene. Earth and Planet. Sci. Lett., 136: 495-510.

Hurrell, J.W., 1995. Decadal trends in the North Atlantic Oscilla- tion: regional temperatures and precipitation. Science, 269: 676-679.

Imbrie, J., Berger., Boyle, E.A., Clemens, S.C., Duffy, A., Howard, W.R., Kukla, G., Kutzbach, J., Martinson, D.G., McIntyre, A., Mix, A.C., Molfino, B., Morley, J.J., Peterson, L.C., Pisias, N.G., Prell, W.L., Raymo, M.E., Shackleton, N.J. and Toggw., 1993. On the structure and origin of major glaciation cycles. Paleoceanography(8(6)): 699-735.

Imbrie, J., Hays, J.D., Martinson, D.G., McIntyre, A., Mix, A.C., Morley, J.J., Pisias, N.G., Prell, W.L. and Shackleton, N.J., 1984. The orbital theory of Pleistocene climate: Support from a revised chronology of the marine d18O record. In: A.L. Berger, J. Imbrie, J. Hays, G. Kukla and B. Saltzman (Editors). Milankovitch and Climate. D. Reidel, Dordrecht, pp. 269-305.

Kaouras, G., 1989. Kohlepetrographische, palynologische und sedimentologische Untersuchungen der pliozänen Braunkohle von Kariochori bei Ptolemais/NW-Griechenland. PhD Thesis, Georg-August-Universität, Göttingen, 258 pp.

Kloosterboer-van Hoeve, M.L., Steenbrink, J., Visscher, H. and Brinkhuis, H., 2006. Millennial-scale climatic cycles in the Early Pliocene pollen record of Ptolemais, northern Greece. Palaeogeogr. Palaeoclimatol. Palaeoecol., 229: 321-334.

Krijgsman, W., Hilgen, F.J., Langereis, C.G., Santarelli, A. and Zachariasse, W.J., 1995. Late Miocene magnetostratigraphy, biostratigraphy and cyclostratigraphy in the Mediterranean. Earth Planet, Sci. Lett., 136.

Krijgsman, W.F., Hilgen, J., Raffi, I., Sierro, J. and Wilson, D.S., 1999. Chronology, causes and progression of the Messinian salinity crisis. Nature, 400: 625-655.

Kuiper, K.F., 2003. Direct intercalibration of radio-isotopic and astronomical time in the Mediterranean Neogene. PhD Thesis, Utrecht University, Utrecht, 223 pp.

Langereis, C.G. and Hilgen, F.J., 1991. The Rossello composite: a Mediterranean and global reference section for the Early to early Late Pliocene. Earth Planet. Sci. Lett., 104: 211-225.

Laskar, J., Robutel, P., Joutel, F., Gastineau, M., Correia, A.C.M. and Levrard, B., 2004. A long-term numerical solution for the insolation quantities of the Earth. Astronomy and Astrophysics, 428: 261-285.

Lomb, N.R., 1976. Least-squares frequency analysis of unequally spaced data. Astrophysics and Space Science, 39: 447-462.

Milankovitch, M., 1941. Kanon der Erdbestrahlungen und seine Anwendung auf das Eiszeitenproblem, Belgrad, 633 pp.

Mudelsee, M. and Raymo, M.E., 2005. Slow dynamics of the Northern Hemisphere glaciation. Paleoceanography, 20: 1-14.

Paillard , D., Labeyrie, L. and Yiou, P., 1996. AnalySeries 1.0a5.

Papakonstantinou, A., 1979. Die hydrogeologischen Verhältnisse im Raum der Ptolemais-Senke und des westlichen Vermiongebirges in Griechisch-Makedonien. Berliner Geowissenschaftliche Abhandlung, 13: 1-79.

Pavlides, S.B. and Mountrakis, D.M., 1987. Extensional tectonics of northwestern Macedonia, Greece, since the late Miocene. J. Struct Geol., 9(4): 385-392.

Robinson, A.R., Garrett, C.J., Malanotte-Rizzoli, P., Manabe, S., Philander, S.G., Pinardi, N., Roether, W., Schott, F.A. and Shukla, J., 1993. Mediterranean and global ocean and climate dynamics. EOS, 74(44): 506-507.

Ruddiman, W., 2004. The Role of Greenhouse Gases in Orbital-Scale Climatic Changes. Eos, 85(1): 6-7.

Scargle, J.D., 1982. Studies in astronomical time series analysis. II. Statistical aspects of spectral analysis of unevenly spaced data. The Astrophysical Journal, 263: 835-853.

Scargle, J.D., 1989. Studies in astronomical time series analysis. III. Fourier transforms, autocorrelation functions, and cross-correlation functions of unevenly spaced data. The Astrophysical Journal, 343(133): 874-887.

Schulz, M. and Mudelsee, M., 2002. REDFIT: estimation red-noise spectra directly from unevenly spaced paleoclimatic time series. Computer & Geosciences, 28: 421-426.

Steenbrink, J., Hilgen, F.J., Krijgsman, W., Wijbrans, J.R. and Meulenkamp, J.E., 2006. Late Miocene to Early Pliocene depositional history of the intramontane Florina-Ptolemais-Servia Basin, NW Greece: Interplay between orbital forcing and tectonics. Palaeoecology, 238: 151-178.

Steenbrink, J., Kloosterboer-van Hoeve, M.L. and Hilgen, F.J., 2003. Millennial-scale climate variations recorded in Early Pliocene colour reflectance time series from the lacustrine Ptolemais Basin (NW Greece). Global and Planetary Change, 36: 47-75.

Steenbrink, J., van Vugt, N., Hilgen, F.J., Wijbrans, J.R. and Meulenkamp, J.E., 1999. Sedimentary cycles and volcanic ash beds in the Lower Pliocene lacustrine succession of Ptolemais (NW Greece): discrepancy between 40Ar/39Ar and astronomical ages. Palaeogeography, Palaeoclimatology, Palaeoecology, 152: 283-303.

Steenbrink, J., van Vugt, N., Kloosterboer-van Hoeve, M.L. and Hilgen, F.J., 2000. Refinement of the Messinian APTS from sedimentary cycle patterns in the lacustrine Lava section (Servia Basin, NW-Greece). Earth and Planetary Science Letters, 181: 161-173.

Stocker, T.F., 1998. The seesaw effect. Science, 282: 61-62.

Sun, J. and Huang, X., 2006. Half-precessional cycles recorded in Chinese loess: response to low-latitude insolation forcing during the Last Interglaciation. Quaternary Sci. Res., 25: 1065-1072.

Tiedemann, R., Sarnthein, M. and Shackleton, N.J., 1994. Astronomic timescale for the Pliocene Atlantic d18O and dust flux records- of Ocean Drilling Program site 659. Paleoceanography(9(4)): 619-638.

Tougiannidis, N., 2009. Karbonat- und Lignitzyklen im Ptolemais-Becken: Orbitale Steuerung und suborbitale Variabilität (Spätneogen, NW Griechenland). Sedimentologische Fallstudie unter Berücksichtigung gesteinsmagentischer Eigenschaften. Monography Thesis, University of Cologne, Cologne, 122 pp.

van de Weerd, A., 1983. Palynology of some upper Miocene and Pliocene Formations in Greece. Geologisches Jahrbuch, 48: 3-63.

van Vugt, N., Langereis, C.G. and Hilgen, F.J., 2001. Orbital forcing in Pliocene - Pleistocene Mediterranean lacustrine deposits: dominant expression of eccentricity versus precession. Paleogeography, Paleoclimatology, Paleoecology, 172: 193-205.

van Vugt, N., Steenbrink, J., Langereis, C.G., Hilgen, F.J. and Meulenkamp, J.E., 1998. Magnetostratigraphy-based astronomical tuning of the early Pliocene lacustrine sediments of Ptolemais (NW Greece) and bed-to-bed correlation with the marine record. Earth and Planetary Science Letters, 164: 535-551.

Velitzelos, E. and Gregor, H.J., 1990. Some aspekts of the Neogene floral history in Greece. Review of Palaebotany and Palynology, 62: 291-307.

Vollmer, T., Ricken, W., Weber, M.E., Tougiannidis, N., Röhling, H.-G. and Hambach, U., 2008. Orbital control on Upper Triassic Playa cycles of the Steinmergel-Keuper(Norian): A new concept for ancient playa cycles. Paleogeography, Paleoclimatology, Paleoecology, 267: 1-16.

Weber, M.E., 1998. Estimation of biogenic carbonate and opal by continuous non-destructive measurements in deep-sea sediments: application to the eastern Equatorial Pacific. Deep-Sea Research 1, 45: 1955-1975.

Weber, M.E., Fenner, J., Thies, A. and Cepek, P., 2001. Biological response to Milankovitch forcing during the Late Albian (Kirchrode I borehole, northwestern Germany). Palaeogeography, Palaeoclimatology, Palaeoecology, 174: 269-286.

Zijderveld, J.D.A., 1967. A.C. demagnetization of rocks: analysis of results. In: D.W.e.a. Collinson (Editor). Elsevier, Amsterdam, pp. 254-286.

Figure 1
Click here to download high resolution image

Fig. I

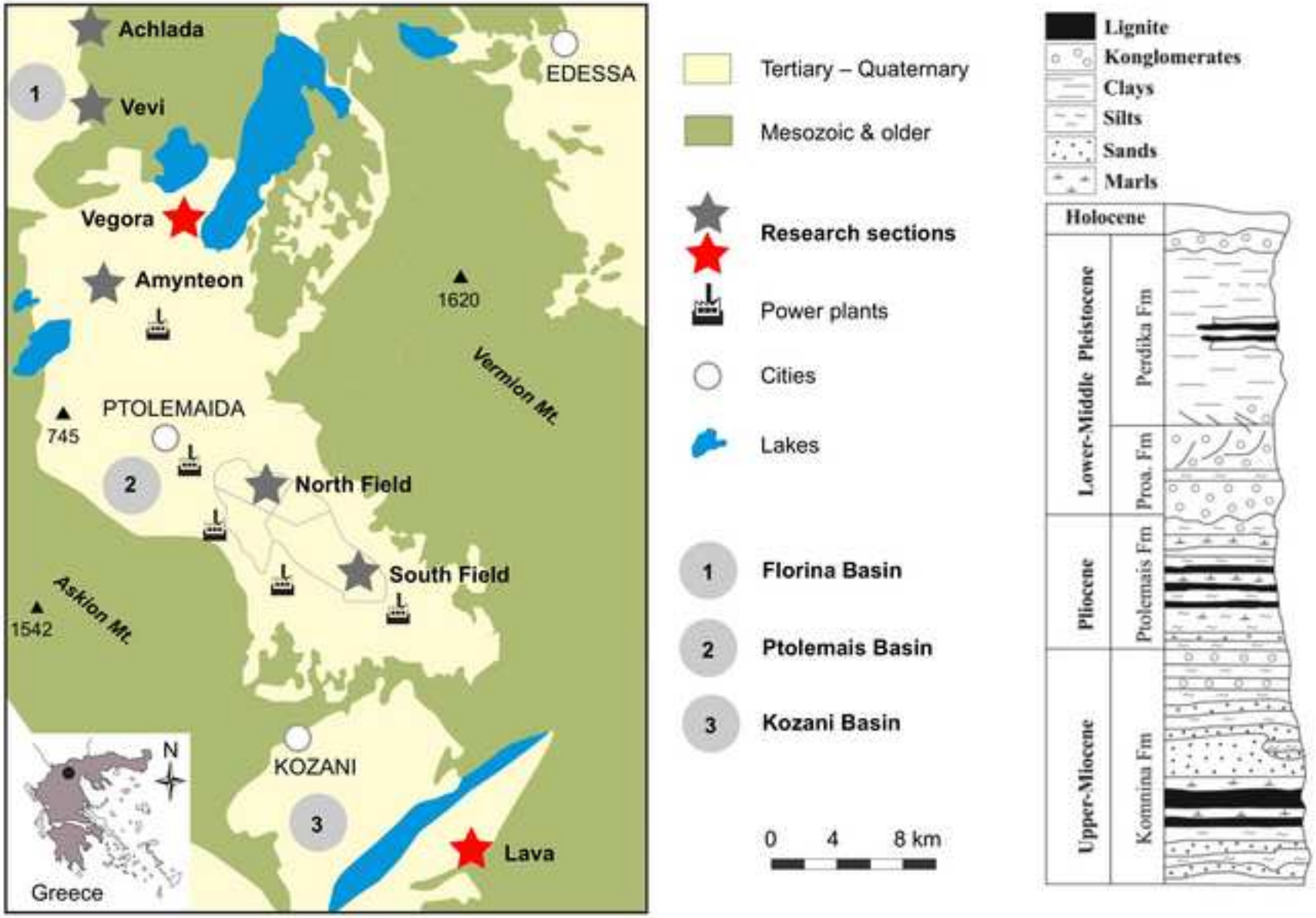

Figure 2
Click here to download high resolution image

Fig. 2

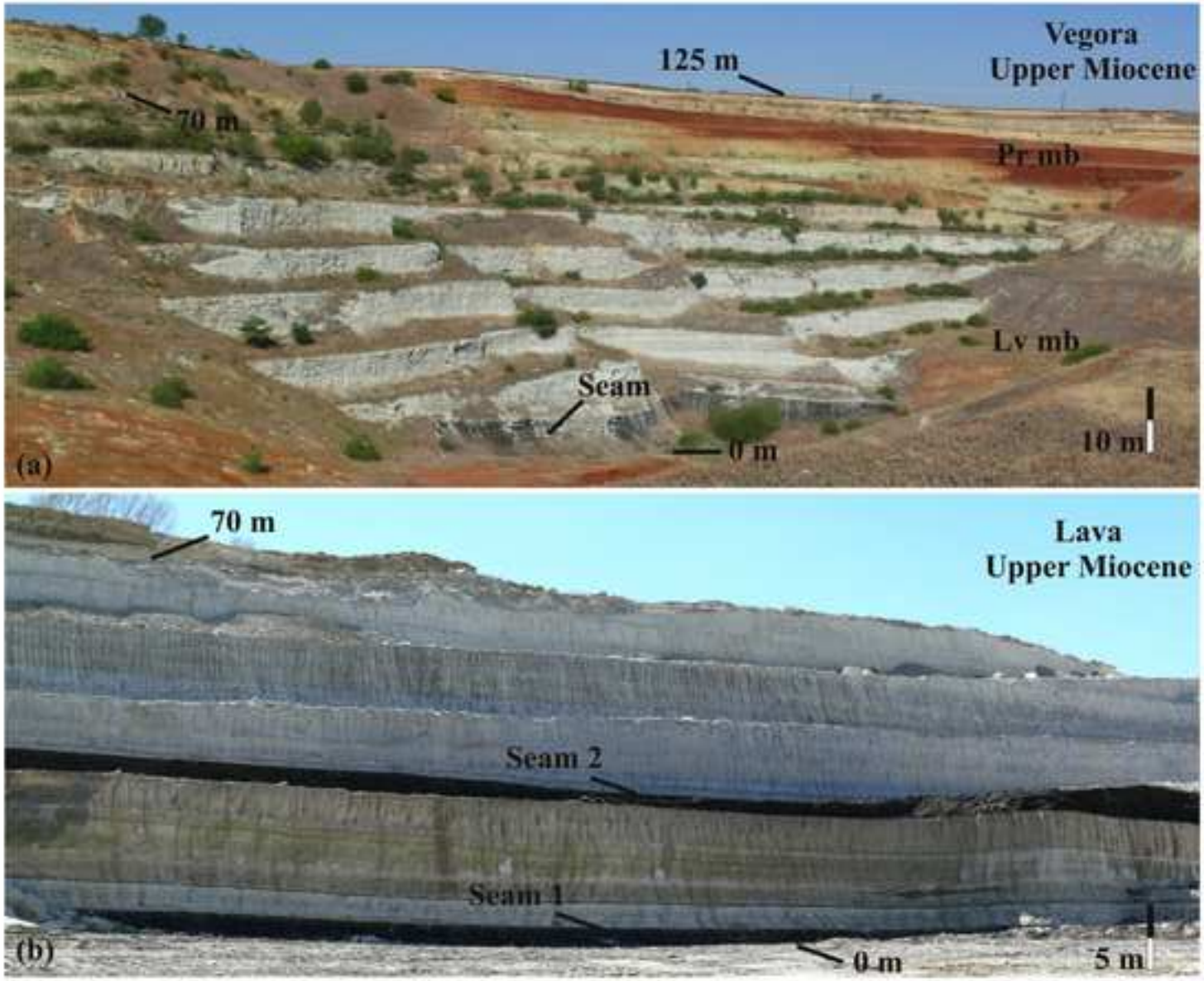

Figure 3
Click here to download high resolution image

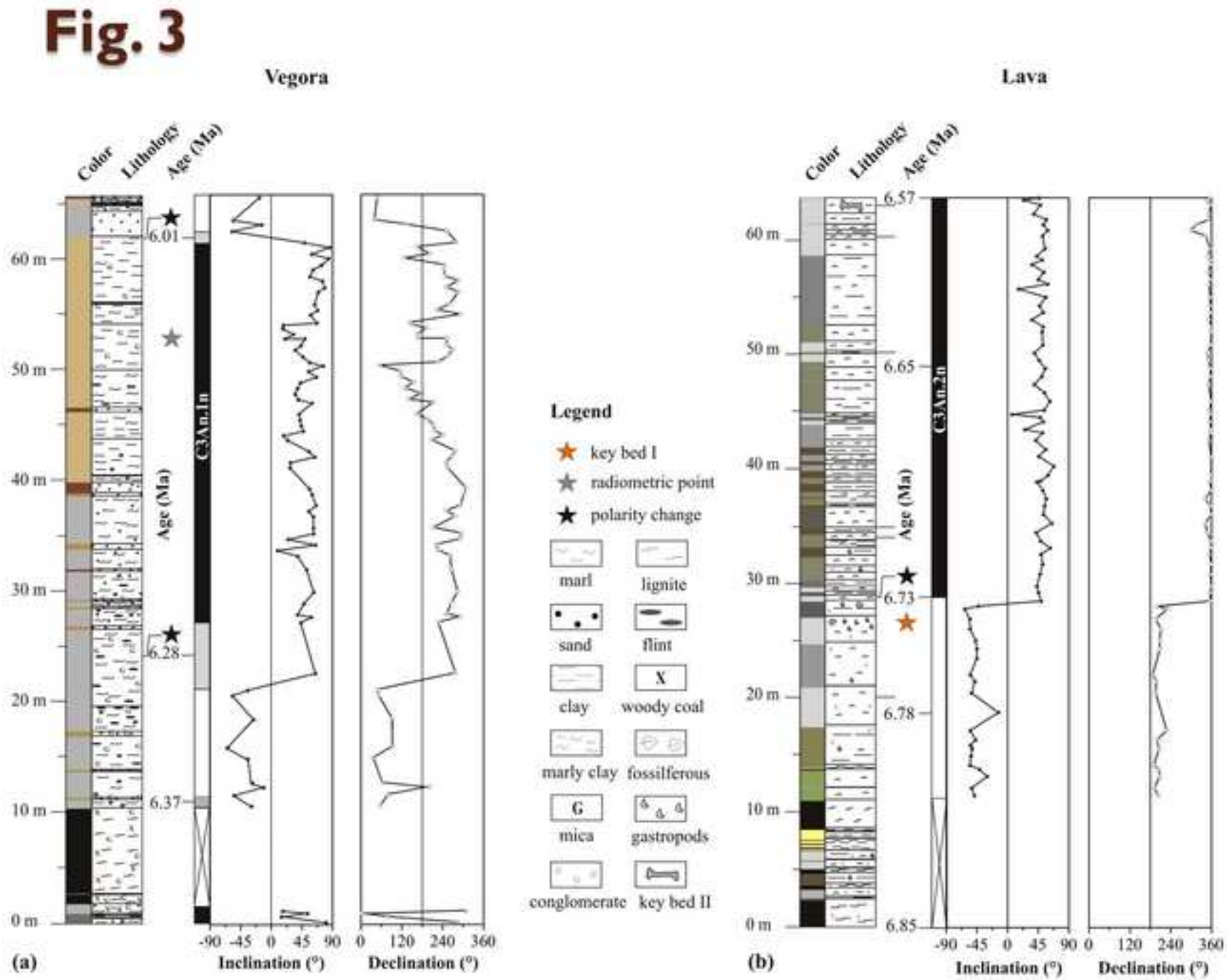

Figure 4
Click here to download high resolution image

Fig. 4

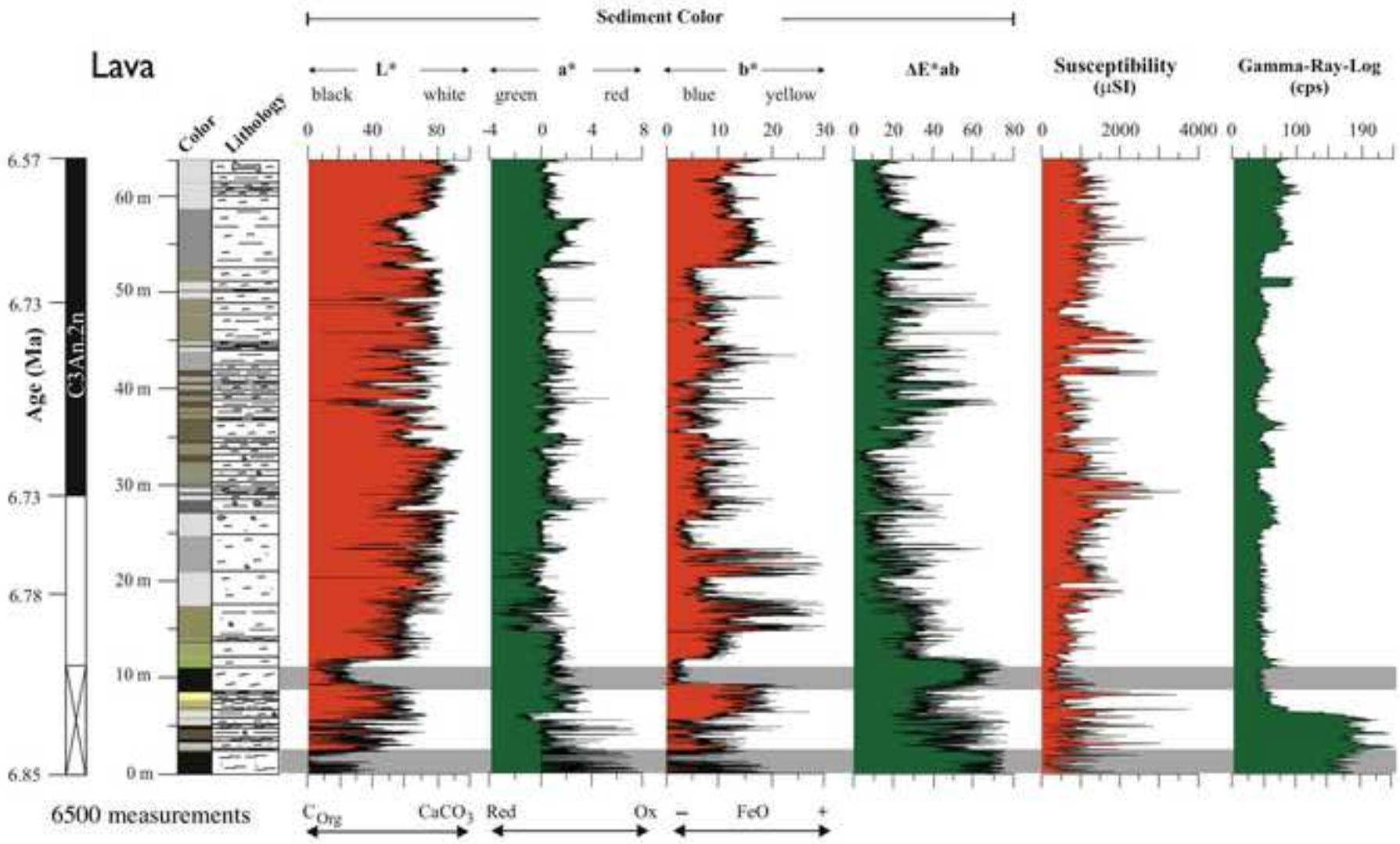

Figure 5
Click here to download high resolution image

Fig. 5

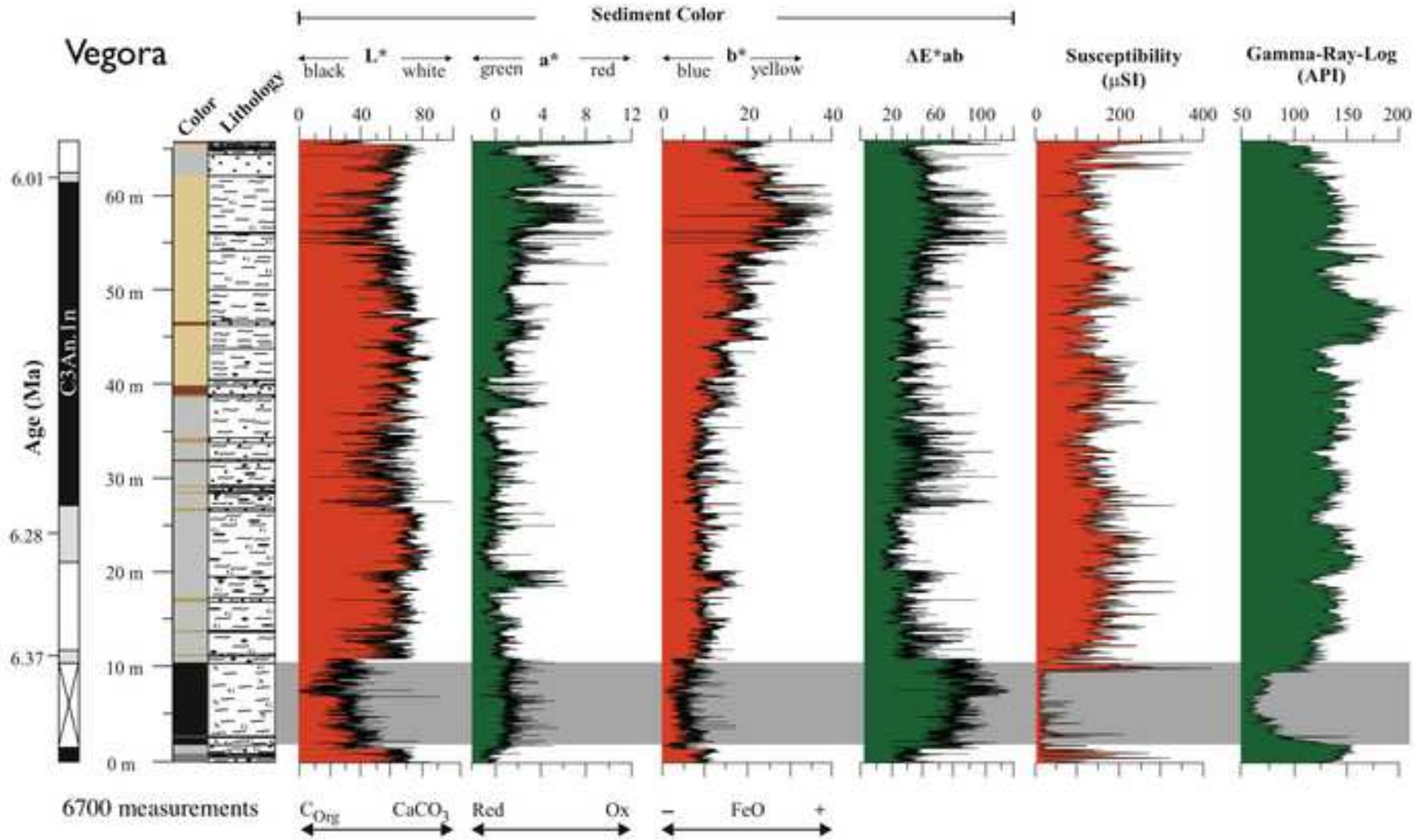

Figure 6
Click here to download high resolution image

Fig. 6

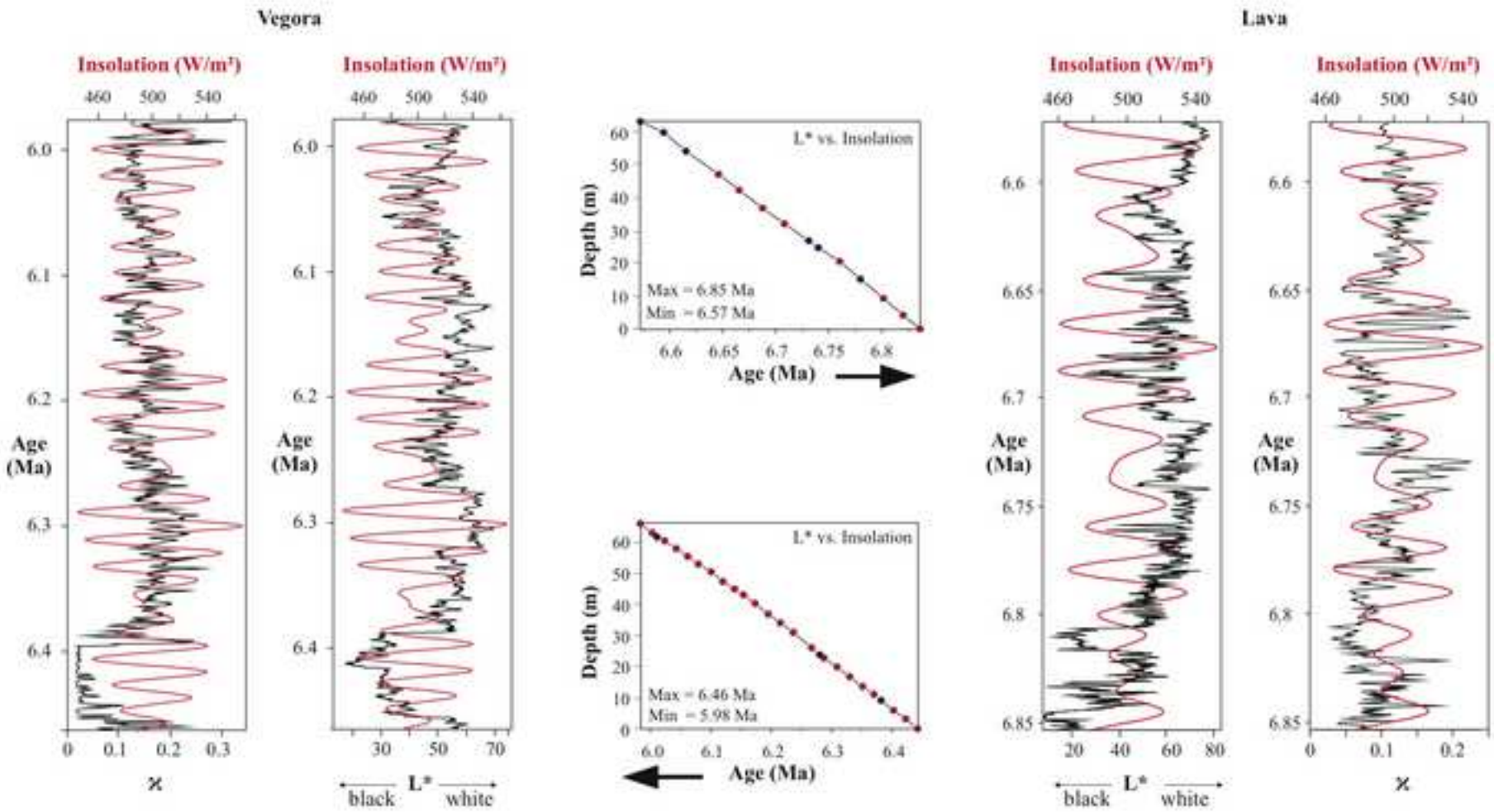

Figure 7
Click here to download high resolution image

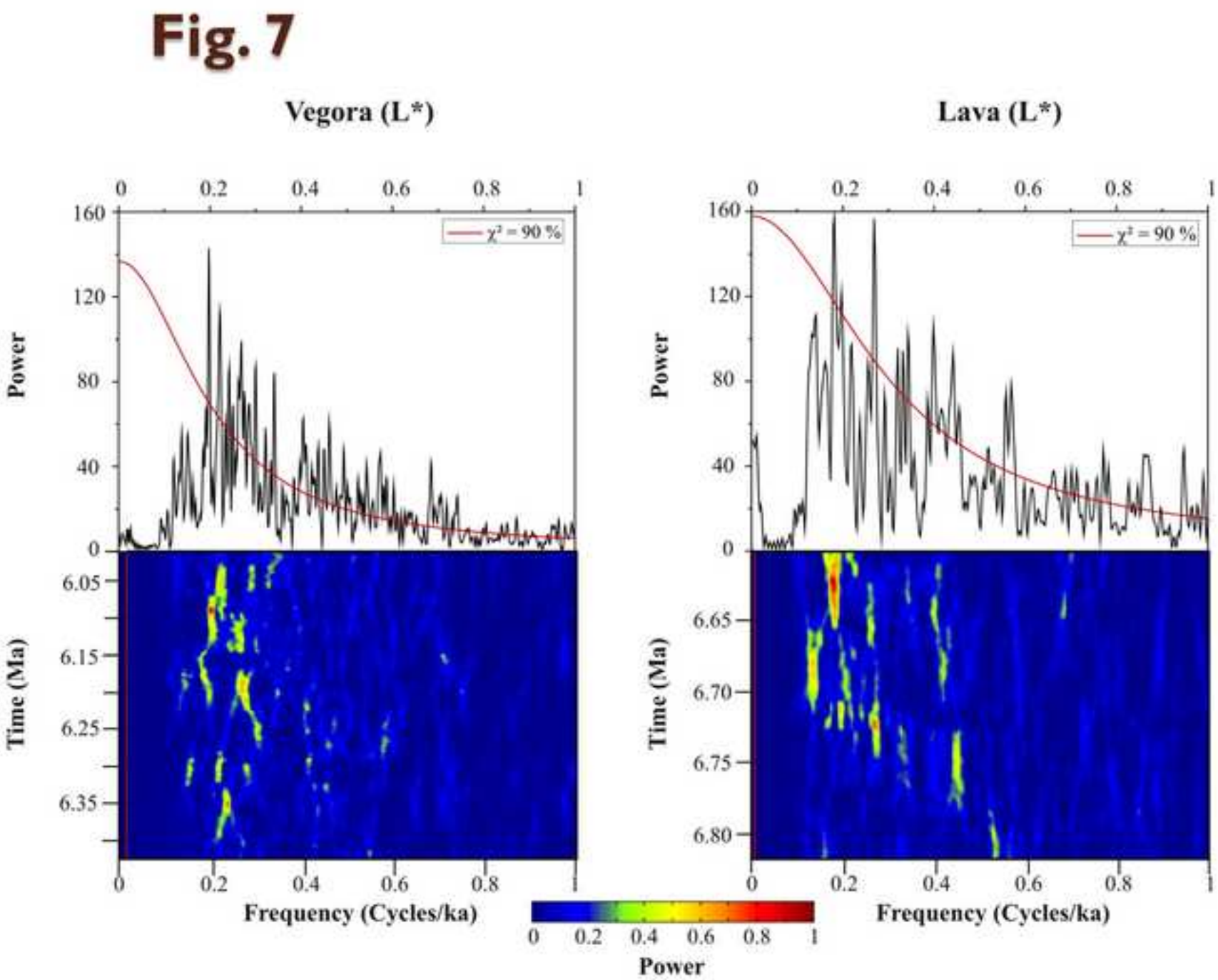

Figure 8
Click here to download high resolution image